

# Rearrangement collisions between gold clusters<sup>?</sup>

Jose Rogan<sup>1</sup>, Ricardo Ramirez<sup>2</sup>, Aldo H. Romero<sup>2</sup>, and Miguel Kwi<sup>2</sup>

<sup>1</sup> Departamento de Física, Facultad de Ciencias, Universidad de Chile, Casilla 653, Santiago 1, CHILE

<sup>2</sup> Facultad de Física, Universidad Católica de Chile, Casilla 306, Santiago, CHILE 6904411

Received: date / Revised version: date

**Abstract.** Collision processes between two gold clusters are investigated using classical molecular dynamics in combination with embedded atom (EA) potentials, after checking the reliability of EA results by contrasting them with first principles calculations. The Au projectiles considered are both single atoms ( $N=1$ ) and clusters of  $N=2, 12, 13$  and  $14$  atoms. The targets contain  $N=12, 13$  and  $14$  gold atoms. The initial projectile energy  $E$  is in the range  $0 < E < 1.5$  eV/atom. The results of the collision processes are described and analyzed in detail.

PACS. 36.40.Qv Stability and fragmentation of clusters {

36.40.Mr Spectroscopy and geometrical structure of clusters {

61.46.+w Nanoscale materials: clusters, nanoparticles, nanotubes, and nanocrystals {

73.22.-f Electronic structure of nanoscale materials: clusters, nanoparticles, nanotubes, and nanocrystals {

82.30.Nr Association, addition, insertion, cluster formation

## 1 Introduction

The study of nanostructures has recently attracted widespread interest among theoretical and experimental physicists and chemists, and because of its many applications

has also come to the forefront of technology [1]. On the theoretical side *ab initio* procedures are now capable of providing incisive insights into the properties of these systems. In addition, novel and sophisticated nanostructure fabrication, manipulation and measurement techniques have given impetus to experiment, and reliability to a large amount of experimental data [2,3,4,5,6,7]. Moreover, the technological applications on a variety of devices has strongly

Send o print requests to: Miguel Kwi

<sup>?</sup> Supported by the Fondo Nacional de Investigaciones Científicas y Tecnológicas (FONDECYT, Chile) under grant

stimulated activity in the nanostructure field since they can be considered as building blocks of novel nanostructured materials and devices [8,9,10,11].

In particular, metallic clusters provide an interesting subject of study for at least two reasons: i) clusters constitute intermediate systems between isolated atoms and molecules, on the one extreme, and bulk solids on the other (i.e. they constitute genuine mesoscopic systems); and ii) often they exhibit an interesting phenomenology of their own. Gold clusters have received widespread attention during the last two decades, both experimentally [2,3,4,5,6,7] and theoretically [12,13,14,15,16,17,18,19,20,21,22,23,24,25].

In principle one does expect *ab initio* procedures to be the definitive tool to handle this type of systems; however, it is not always feasible (or at least practical) to implement *ab initio* calculations. In fact, since we are interested in structures with a fairly large number of atoms, or arranged in several different interacting nanostructures, *ab initio* computations first become very time consuming and, in the end, in practical. Much the same happens when attempting to obtain a detailed description of the long time evolution of small systems, or to describe their properties when subject to a large variety of external conditions.

Here we intend to develop an adequate description of colliding gold clusters, a phenomenon which falls into one or more of the categories described in the preceding paragraph. In this paper we employ mainly classical molecu-

lar dynamics [20]. Classical molecular dynamics (MD) is a valid option in this case, since it allows to considerably reduce the computation time (relative to MD *ab initio* calculations), and/or to increase substantially the number of particles that can be handled. Obviously, there is a price to pay; as examples of this cost we mention that the method is at best semi-classical, that the detailed electronic structure is ignored, and that phenomenological potentials, adjusted to bulk properties, are used. In spite of these shortcomings the MD technique can reliably be used to compute the properties dominated by the ionic contribution, which is the case for the phenomena treated in this paper. This is especially true when MD is checked, in some physical limit, against first principle calculations. An alternative, but equally convenient procedure, is to close in on a solution, for example for geometrical optimization via MD, to be followed by first principle calculations. The synergy between *ab initio* and MD thus allows to significantly reduce the resources that are required and to expand the set of problems amenable to treatment.

More than a decade ago the bombardment with gold clusters of metallic surfaces was investigated experimentally [26] and theoretically [27,28,29]. Moreover, the dramatic energy accommodation that occurs in cluster-cluster collisions, which is crucial to understand the growth mechanism during the early stages of particle formation, was investigated around the same time by Blastein et al. [30]. We focus our interest on the dynamics of gold cluster colli-

of small Au clusters, and the dynamics of atom-cluster and cluster-cluster collisions, for different values of the impact parameter  $b$  and as a function of center of mass energy  $E$ .

This paper is organized as follows: after this Introduction we describe, in Sec. 2, both the *ab initio* and EA methods employed in the computations. In Sec. 3 we provide results, for a large variety of cases, of the implementation of the codes, for the cluster structures, their symmetries and the dynamics of the collision process. Finally, in Sec. 4 we draw conclusions and close the paper.

## 2 Simulation method

### 2.1 Ab-initio method

In order to assess the quality of the semi-empirical embedded atom (EA) procedure used in the context of our classical molecular dynamics simulations, we start contrasting EA against first principles calculations. Thus, *ab initio* geometrical optimization was carried out within the Car-Parrinello approach [31], in the framework of the density functional theory, using gradient corrections in the PBE implementation [32]. Gradient corrected functionals have been adopted in recent theoretical studies of geometrical optimization of metallic clusters, mainly because they are more accurate than the local density functional, even though there still is some controversy in the literature on the ground state geometry of small Au clusters [15, 33, 34]. The calculations were performed only at the  $\Gamma$ -point

[35]. The wavefunctions were expanded in plane waves, with an energy cutoff of 60 Ry. We have explicitly checked that, with this energy cutoff, the structural properties of our system are well converged. The box used in the calculations was always at least three times larger than the cluster diameter. The results obtained, as well as their EA counterparts, are given in Fig. 2 and in Table 4. The *ab initio* optimized geometries are illustrated in Fig. 1. The agreement between *ab initio*, EA and Wilson and Johnston [21] (WJ) procedures is quite satisfactory for large clusters ( $N \geq 10$ ) and provides a reasonable basis to trust the EA calculations that constitute the core of the present paper.

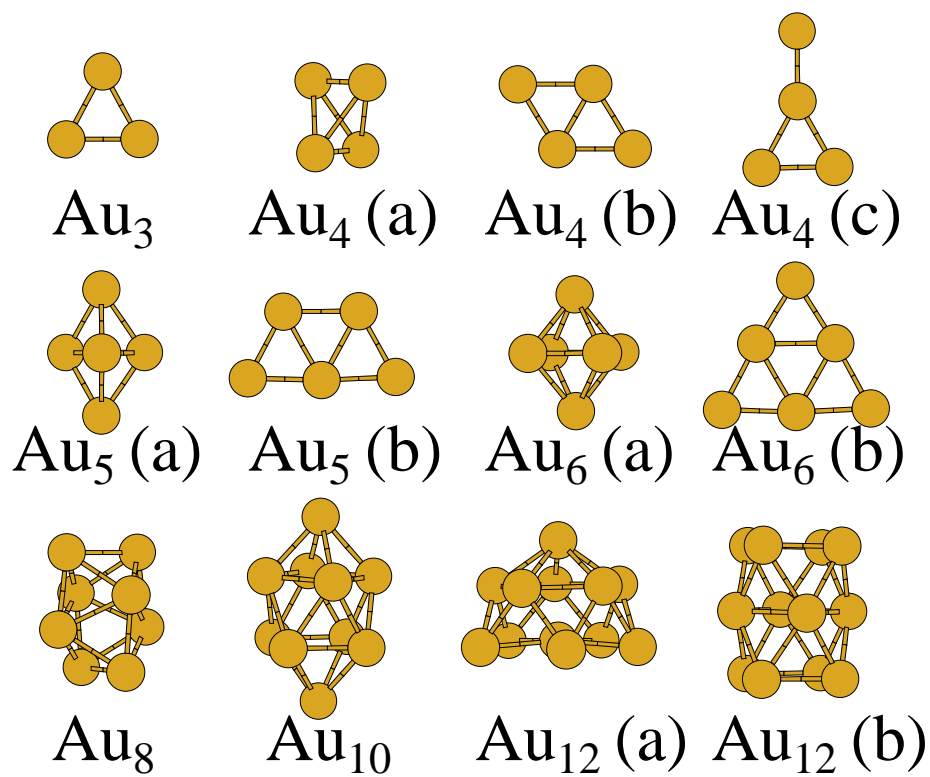


Fig. 1. Ab initio optimized geometries for 3, 4, 6, 8, 10 and 12 atom gold clusters.

## 2.2 Embedded atom method

The interatomic interaction between gold atoms is modeled using a semi-empirical (EA) potentials [36,37]. On the basis of these EA potentials we obtain the average binding energy per atom,  $E_b$ , which is later minimized to yield the optimal cluster geometry. The latter is achieved using a Monte Carlo procedure, for which we adopted as starting configurations, for the different cluster sizes, the geometries found by Wilson and Johnston [21] (WJ). Once the optimal geometry is established several static properties, like nearest neighbor distances and angles, and the average coordination number, are readily evaluated.

After the various different clusters are properly characterized we use classical molecular dynamics (MD) to simulate the cluster-cluster scattering process. Many body EA semi-empirical potentials are used throughout. To integrate the equations of motion we implement the Verlet velocity algorithm, with a 1 femtosecond time step. Since the collision fragments heat up as a consequence of the scattering process it is necessary to cool them down; to do so we simply rescale the temperature by 1 % every 1000 steps, during a total of 100 000 time steps, to reach a final energy of 63 % of the initial one. Finally, the collision fragments are carefully scrutinized to extract the physical information we are looking for.

## 3 Results and Discussion

### 3.1 Structures

The first issue we address is to check the reliability of our MD procedure as compared with alternative methods. In Table 4 we compare the average binding energy  $E_b$  of the lowest energy configurations, and the average nearest neighbor distance  $R$ , of clusters built with different numbers of Au atoms. On the one hand we have *ab initio* results obtained within the framework of density functional theory, and on the other the empirical potential results of WJ [21] (who used the Murrell-Motttram [38,39] potential) as well as the EA values that we obtained.

It is quite apparent that the EA estimates for  $E_b$  differ considerably from the ones found by WJ, and also with the more trustworthy *ab initio* results. However for small clusters the geometrical parameters are not so satisfactory. This small  $N$  (where  $N$  is the number of atoms in the cluster) error margin is not unexpected, since the EA potential has been adjusted to bulk properties and cannot be expected to fully succeed in systems where  $N$  is tiny. However, and also as expected, the situation improves as  $N$  increases, which is precisely what is borne out by Table 4, where we display results for the range of cluster sizes from  $N = 3$  to 12. The same trend is observed in Fig. 2, where we plot  $E_b$  versus  $N$ . We notice that *ab initio* calculations were performed for  $N = 4, 5$  and 6 planar and three dimensional structures. It is apparent that as the cluster size increases, specially when the number of atoms is larger than 10, that both the *ab initio* and EA values

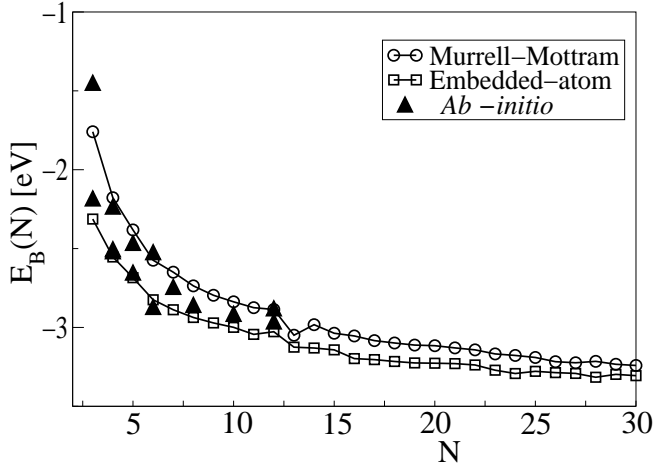


Fig. 2. Binding energies per atom  $E_b$ , obtained by W J using the Murrell-Mottram potential, and by us on the basis of the EA potential and ab initio, as a function of the number of atoms in the cluster  $N$ . The ab initio results, for which we have considered several possible geometries, are detailed in Table 4.

The average nearest neighbor distances  $R$  that we compute also exhibit larger errors than those of W J. In spite of the fact that we employ the W J cluster configurations as the starting point for our calculations, but in which we use a binding energy obtained from a different potential, we derive geometrical structures which differ from those of W J. However, once again, increasing  $N$  yields compatible results. For example, for a 3-atom cluster the difference in nearest neighbor distances amounts to 15%, but already for a 6-atom cluster it reduces to only 8%. These average distances are illustrated in Fig. 3, where we plot  $R$  as a function of the number of atoms in the cluster,  $N$ . In contrast with Fig. 2 the plot of Fig. 3 is not smooth, but shows abrupt variations between two successive values of  $N$ . Despite this roughness the tendency of the W J and our

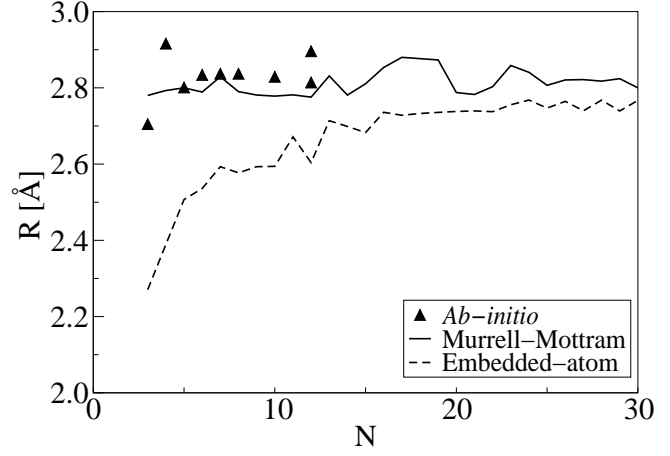


Fig. 3. Average nearest neighbor distances  $R$  calculated using EA (dashed line), and those obtained by W J using the Murrell-Mottram potential (full line).

our results are in good agreement with the ab initio ones obtained by Wang [16].

### 3.2 Symmetries

In addition to the binding energies and interatomic distances the cluster symmetry is a relevant characteristic and, in the context of gold cluster topologies, the Jahn-Teller effect is also an important element. Ab initio calculations predict a  $C_{2v}$  symmetry for  $Au_3$  and  $Au_4$ , while EA yields  $C_{2v}$  and  $D_{2d}$ , and the Murrell-Mottram potential used by W J yields  $D_{3h}$  and  $T_d$  symmetries, respectively. These differences are quite apparent in the pair correlation function  $g(r)$  plotted in Fig. 4.

The second difference in the binding energy is defined by

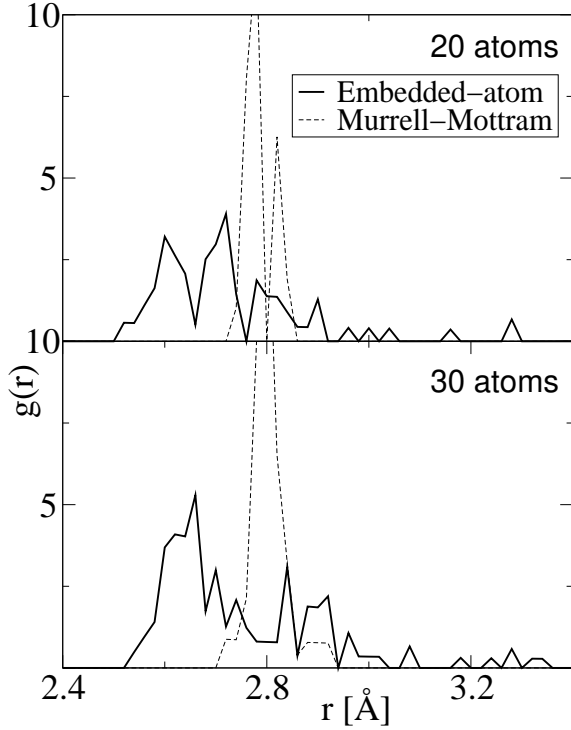


Fig. 4. Pair correlation function  $g(r)$  for 20, 30 and 40 Au atom clusters as calculated by us, using EA potentials, and by W J.

and gives an indication of the stability of a cluster with respect to disproportionation [1], as well as its ionic hardness. A plot of  $\Delta_2 E_b(N)$  as a function of  $N$  is given in Fig. 5, where we observe a good agreement of our EA values with those reported by Wilson et al. [21], both for the position and magnitude of the hardness peaks. The maxima (minima) of  $\Delta_2 E_b(N)$  imply that there are values for which it is more difficult (easier) to add an atom to the cluster. Moreover, as  $N \rightarrow 1$  the plot becomes quite smooth, which constitutes an indication that the cluster can incorporate an additional atom without major hindrance.

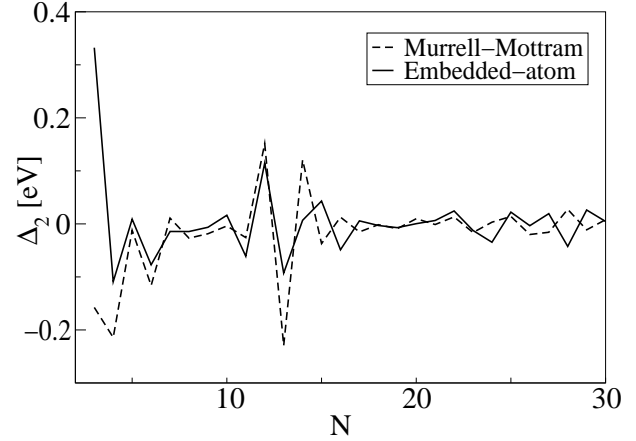


Fig. 5. Second difference in the binding energy  $\Delta_2 E_b(N)$  as a function of cluster size  $N$ .

### 3.3 Collisions between a single Au atom and a Au cluster

Next we report the results of our simulations of the collisions between a single Au atom and a variable size Au cluster, for several values both of the initial per atom energy  $E$  and of the impact parameter  $b$ . The precise details that describe the collision process are as follows: at time  $t = 0$  the centers of mass of the atom and the cluster are placed along the  $x$ -axis,  $10\text{\AA}$  away from the origin, respectively. The atom is located a distance  $b$  away from the  $x$ -axis, along the  $y$ -axis on the  $xy$  plane. The principal symmetry axes of the various clusters are aligned perpendicular to the direction of motion, that is parallel to  $y$ . The impact parameter  $b$  is varied between 0 (head-on collision) and  $7\text{\AA}$ ; the latter corresponds to the distance where the interaction potential effectively vanishes, since the average radius of a cluster with  $12 \leq N \leq 14$  is less than  $3\text{\AA}$  and

varied between 0.1 and 1.5 eV per atom, in steps of 0.2 eV (8 values in all). The maximum energy  $E = 1.5$  eV per atom corresponds to approximately one half of the cluster binding energy. After the collision takes place the resulting fragments are stabilized, by gradual cooling through the rescaling of the internal velocities. Finally, we analyze the data characterizing the collision fragments for several special cases.

We consider two categories: i) the scattering of a single gold atom against clusters with  $N = 12, 13$  and 14 atoms, which is dealt with here; and, ii) the scattering of a variable size projectile ( $N = 12, 13$  y 14) on a variable size target with a similar number of Au atoms, which is presented in 3.4. Throughout we use the concepts of low and high energies, and small and large impact parameters. Low energies are defined to be in the range  $0.1 \leq E \leq 0.7$  eV and large within  $0.7 \leq E \leq 1.5$  eV. Similarly, small impact parameters cover the range  $0 \leq b \leq 3\text{Å}$ , and large is defined as  $3 \leq b \leq 7\text{Å}$ . The upper bounds on  $E$  and  $b$ , as mentioned above, are related to the binding energy of the cluster and the distance at which the projectile does not interact with the target, respectively.

One atom on 12 Because of the rich variety of results, and to facilitate their understanding by the reader, we have chosen to illustrate them by means of figures. In particular Fig. 6 describes the one gold atom collision with a 12 atom cluster. In this and ensuing figures the columns correspond to different values of the energy per atom (in eV), while the rows correspond to several different impact

on the basis of the following symbols: single atoms, dimers and trimers are represented by dots, two dots joined by a line, and three dots that form a triangle, respectively. When several of these collision fragments are generated we denote their number by a factor in front of the corresponding symbol. If the fragment contains four or more atoms the symbolic representation is a circle. Finally, if the number of atoms in the target is not altered after the collision, we stress this fact representing it by a square with the original number of target atoms in its interior, as long as  $N \geq 4$ .

In Fig. 6 it is noticed that for low energies and small impact parameter ( $0 \leq b \leq 3\text{Å}$ ), projectile and target fuse into a 13 atom cluster. When the energy is increased to  $0.9 \leq E \leq 1.5$  eV, keeping the impact parameter fixed, coalescence is observed for a few cases, while more often 11 or 9 atom clusters, and one or two dimers, respectively, are generated. For larger impact parameters,  $4 \leq b \leq 7$ , fusion is present in the low energy region, but for a few cases target and projectile remain unaltered. Finally, for large  $b$  and  $E$  values we observe a few cases of coalescence, some 11 atom clusters plus a dimer and many instances (denoted by squares) in which projectile and target size do not change.

A particularly interesting scattering process, illustrated in Figs. 7, occurs for an energy of 4 eV and impact parameter  $1.8 < b < 2.2\text{Å}$ . When the projectile approaches the target (Fig. 7a) it attracts the nearest (lowest in Fig. 7b) atom, but without removing it from the cluster. This gen-



|   | 0.1 | 0.3 | 0.5  | 0.7  | 0.9  | 1.1  | 1.3  | 1.5  |
|---|-----|-----|------|------|------|------|------|------|
| 0 | ⑬   | ⑬   | ⑬    | ⑬    | ⑬    | ⑬    | ⑪ 1• | ⑪ 1• |
| 1 | ⑬   | ⑬   | ⑬    | ⑬    | ⑬    | ⑪ 1• | ⑪ 1• | ⑬    |
| 2 | ⑬   | ⑬   | ⑬    | ⑬    | ⑬    | ⑬    | ⑬    | ⑨ 2• |
| 3 | ⑬   | ⑬   | ⑬    | ⑬    | ⑬    | ⑪ 1• | ⑪ 1• | ⑪ 1• |
| 4 | ⑬   | ⑬   | ⑬    | ⑬    | ⑪ 1• | ⑬    | ⑪ 1• | ⑪ 1• |
| 5 | ⑬   | ⑬   | ⑬    | ⑫ 1• | ⑫ 1• | ⑫ 1• | ⑫ 1• | ⑫ 1• |
| 6 | ⑬   | ⑬   | ⑬    | ⑬    | ⑬    | ⑪ 1• | ⑫ 1• | ⑫ 1• |
| 7 | ⑬   | ⑬   | ⑫ 1• | ⑫ 1• | ⑫ 1• | ⑫ 1• | ⑫ 1• | ⑫ 1• |

Fig. 6. One Au on 12 atom cluster collision. The numbers on the left column denote the impact parameter  $b$ , measured in Å, and the top row the average energy per atom  $E$  in eV.

amplitude vibrations in the "lowest" atom, as the projectile leaves the scene (Fig. 7c). As a consequence of these large amplitude vibrations this particular atom does overcome the energy barrier and ends up at the center of the cluster (Fig. 7c). We have estimated a lower bound for this energy barrier of 0.03 eV. Quite remarkably this lower symmetry cluster has an energy slightly smaller than the fully symmetric 12 atom cluster we accepted above as the stable configuration.

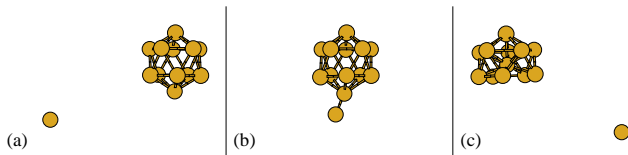


Fig. 7. Collision between a single Au atom and a 12 atom cluster. The single atom approaches the cluster from the left (a), and exchanges energy (b). Finally, in (c) one of the cluster atoms is displaced towards the target center, while the projectile

In fact, the original 12 ( $I_h$ ) cluster has a binding energy  $E_b = 3.03$  eV, while the energy of the less symmetric configuration 12 ( $C_{5v}$ ) equals  $E_b = 3.09$  eV, which is 2% lower. Thus, we are faced with the question of why this lower energy configuration was not obtained in the minimization process we reported above. The explanation of this apparent contradiction is related to the fact that the energy barrier the atom has to overcome, to shift to the center of the cluster, is rather large and cannot be achieved in a minimization process that starts with an icosahedron and allows only small displacements from the original equilibrium positions. It is worth mentioning that this asymmetric structure was also assigned minimum energy by Wilson and Johnston [21]. However, they argue that the bond compression of the 12 ( $C_{5v}$ ) structure generates a repulsion strong enough to destabilize it in favor of the icosahedron.

One atom on 13 When a Au atom collides with the "magic number"  $N = 13$  cluster the results are not much different from the previous 1 on 12 case. However, there is a larger number of coalescence cases, many instances of dimer formation, and also instances are observed where there is no change in the number of atoms of projectile and target. For example, when  $E = 0.9$  eV, there is fusion for  $b = 2$ , dimer plus a 12 atom cluster generation for  $b = 3$ , fusion for  $b = 4$ , no change  $b = 5$ , and fusion for  $b = 6$  and  $b = 7$  Å.

One atom on 14 In this case the results fall into only two categories: either target and projectile fuse or they

For  $b > 5 \text{ \AA}$  there is coalescence only for very small energies  $E \leq 0.3$ , and no change in the number of atoms in projectile and target for larger energies. This small  $b$  large  $E$  behavior can be understood as follows: for low impact parameter the collision gives rise to violent cluster vibrations and deformations, which precludes the trapping of the projectile. Instead, larger  $b$  values induce less drastic cluster deformations and sufficient attraction to fuse projectile and target.

**One atom on 12: cluster rotation** In all preceding cases the cluster symmetry axis was taken to be parallel to the  $y$  axis, that is, perpendicular to the initial projectile velocity. Now we align the cluster symmetry axis parallel to the  $y$  axis. A qualitative change is observed: single atoms as a result of the collision. In fact, for low energies and small  $b$  there is fusion. However, for  $E > 0.7 \text{ eV}$  several alternatives are observed: either coalescence, or 8, 9 and 11 atom cluster formation accompanied by the creation of dimers and single atoms. When  $b > 3 \text{ \AA}$  we obtain 11 atom clusters plus a dimer or a pair of isolated atoms. Finally, for the largest  $b = 7 \text{ \AA}$  value no atomic reordering is observed. However, we notice that in general the overall structure of the results is equivalent to the perpendicularly oriented cluster impact discussed above, which allows us to concentrate on cluster collisions without paying much attention to their relative spatial orientation.

### 3.4 Collisions between two Au clusters

Now we turn to the problem of the collision of two clusters

**One dimer on a 12 atom cluster**

Fusion is obtained for low energies ( $E \leq 0.7 \text{ eV}$ ) and practically all values of the impact parameter  $b$ . In many instances the end result is a dimer and a 12 atom cluster, which are the outcome after a complex dynamic interaction that, finally, yields a reconstruction into the two original clusters. For  $E > 0.7 \text{ eV}$  and small  $b$  we notice a diversity of results: single atoms plus clusters of 5, 6, 7, 8, 10 and 11 atoms are obtained, which reflects the fact that the more complex the projectile the richer the variety of collision fragments.

**One 12 atom cluster on another 12 atom cluster**

Fusion is observed only for low energies ( $E = 0.1 \text{ eV}$  per atom) over the whole range of impact parameters  $0 \leq b \leq 7 \text{ \AA}$ . For large energies and small impact parameter collisions, either large fragments plus a couple of dimers or trimers, or dimers and single atoms are generated. For large  $E$  and large  $b$ , collisions without cluster size rearrangement are predominant.

**One 13 atom cluster on a 12 atom cluster** Again

there is coalescence for  $E \leq 0.1 \text{ eV}$  and  $0 \leq b \leq 7 \text{ \AA}$ , while for large  $E$  and large  $b$  collisions without rearrangement predominate. In the  $0 \leq b \leq 5 \text{ \AA}$  and  $E \leq 0.5 \text{ eV}$  region large and medium size fragments plus trimers, dimers and single atoms are produced. Total break up of the cluster is seen almost exclusively for small  $b$  and large  $E$  collisions.

**One 14 atom cluster on a 12 atom cluster** Again

here the results are quite similar to the previous ones.

For small  $b$  there is fusion, while for large  $b$  and large

clusters. Moreover, for a large region of parameter space ( $0 \leq b \leq 5 \text{ \AA}$  and  $0.5 \leq E \leq 1.5 \text{ eV}$ ) a whole variety of fragments does result: large fragments plus dimers, medium size fragments and finally, in for the largest energies, total cluster breakup into small pieces.

#### One 13 atom cluster on a 13 atom cluster

The collision of two "magic number" clusters yields the rich variety of results illustrated in Fig 8. It is readily noticed that there are many notable exceptions to the general trends observed in the preceding cases, and which are only present for this particular case. This is specially noticeable in the upper right of the figure, which illustrates the parameter values for which dimers, trimers and clusters of 6, 7, 8, 9, 11, 12, 14, 15, 16, 17 and 24 atoms are generated. However, again fusion is observed for low energy collisions ( $E \leq 0.1 \text{ eV}$ ) for all  $b$  values, as well as no rearrangement collisions for large impact parameters, which are the final outcome of a complex dynamic interaction that in the end yields a reconstruction into two clusters equal to the original ones.

#### One 14 atom cluster on a 13 atom cluster

A low energy coalescence region, as well as a large impact parameter zone where after the collision projectile and target rearrange into their original structures, is again obtained. Also, and just as in previous cases, for large  $E$  and small  $b$  a diversity of fragments (dimers, trimers, and 5, 6, 7, 8 and 9 atom clusters) do result. In addition there are several cases with a single Au atom exchange between projectile and cluster, such that the original (14, 13) pair is

|   | 0.1  | 0.3       | 0.5             | 0.7           | 0.9             | 1.1             | 1.3             | 1.5             |
|---|------|-----------|-----------------|---------------|-----------------|-----------------|-----------------|-----------------|
| 0 | (26) | (26)      | (26)            | (24) 2†       | (17) 1†<br>3†   | (11) 1†<br>6†   | (6) 10†         | (4) 7†          |
| 1 | (26) | (26)      | (26)            | (14) 6†       | (14) 6†         | (14) 6†         | 2† 10†          | 2† 10†          |
| 2 | (26) | (26)      | (24) 1†         | (15) 1†<br>4† | (16) 5†         | (8) 9†          | (9) 1†<br>7†    | 2† 10†          |
| 3 | (26) | (26)      | (13) (11)<br>1† | (13) (13)     | (11) (11)<br>2† | (11) (11)<br>2† | (9) (7)<br>5†   | (7) (7)<br>6†   |
| 4 | (26) | (26)      | (26)            | (13) (13)     | (13) (13)       | (11) (11)<br>2† | (13) (11)<br>1† | (13) (11)<br>1† |
| 5 | (26) | (26)      | (26)            | (13) (13)     | (13) (13)       | (13) (11)<br>1† | (13) (13)       | (11) (11)<br>2† |
| 6 | (26) | (26)      | (13) (13)       | (13) (13)     | (13) (13)       | (13) (13)       | (12) (12)<br>1† | (12) (12)<br>1† |
| 7 | (26) | (13) (13) | (13) (13)       | (13) (13)     | (13) (13)       | (13) (13)       | (13) (13)       | (13) (13)       |

Fig. 8. Collision between two 13 atom clusters. The numbers on the left column denote the impact parameter  $b$ , measured in  $\text{\AA}$ , and the top row the average energy per atom  $E$  in eV.

$E$  region when three, instead of two, collision fragments are generated, always a dimer (and not a single atom) is created. This dimer originates in the 14 atom projectile, yielding in the end a 12 atom and a 13 atom cluster plus a dimer, as collision fragments.

## 4 Conclusions

The dynamics of the collision process of gold clusters has been investigated by means of classical molecular dynamics in combination with embedded atom (EA) potentials. First, the reliability of the EA potentials was confirmed by comparison with ab initio values, finding that EA is in good agreement for the cluster sizes we considered, an agreement which improves as  $N$  increases. Next, structural characteristics and the symmetry of the various Au clusters were obtained and contrasted with published re-

Several type collisions were investigated, finding regions of coalescence, fragmentation and scattering. Which of these outcomes actually occurs depends mainly on the values of the projectile energy  $E$  and the impact parameter  $b$ . Coalescence is dominant for low energies ( $E < 0.7$  eV) and small impact parameters ( $b < 3$  Å). Simple scattering, with no change in the size and structure of the colliding clusters, prevails for large  $E$  and  $b$  values. For large energies and small impact parameters fragmentation and scattering are generally the case. For large  $E$  and large  $b$  scattering is the most probable outcome. When the cluster does break up the main collision products, apart from large fragments, are dimers. On the other hand cluster coalescence provides a viable mechanism to generate larger cluster sizes. It is also of interest that the collisions themselves turn out to be rather insensitive to the relative orientation of the projectile and target main symmetry axes, and that cluster collisions can generate metastable structures, which are usually not accessible due to the existence of a potential barrier.

## References

1. W. A. de Heer, *Rev. Mod. Phys.* 65, 611 (1993).
2. C. L. Cleveland, U. Landman, T. G. Schaa, M. N. Shagullin, P. W. Stephens and R. L. Whetten, *Phys. Rev. Lett.* 79, 1873 (1997).
3. T. G. Schaa, W. G. Cullen, P. N. First, I. Vezmar, R. L. Whetten, C. Gutierrez-Wing, J. Asencio and M. J. Jose-Yacamán, *J. Phys. Chem.* 101, 7885 (1997).
4. K. J. Taylor, C. L. Pettiette-Hall, O. Cheshnovsky and R. E. Smalley, *J. Chem. Phys.* 96, 3319 (1992).
5. K. Koga, H. Takeo, T. Ikeda and K. I. Ohshima, *Phys. Rev. B* 57, 4053 (1998).
6. V. A. Spasov, Y. Shi, K. M. Ervin, *Chem. Phys.* 262, 75 (2000).
7. B. Palpant, B. Prevel, J. Leme, E. Cottancin, M. Pellarin, M. Treilleux, A. Perez, J. L. Vialle and M. Broyer, *Phys. Rev. B* 57, 1963 (1998).
8. R. L. Whetten, J. T. Khoury, M. M. Alvarez, S. Murthy, I. Vezmar, Z. L. Wang, P. W. Stephens, C. L. Cleveland, W. D. Luedtke and U. Landman, *Adv. Mater.* 5, 8 (1996).
9. R. P. Andres, T. Bein, M. Dorogi, S. Feng, J. I. Henderson, C. P. Kubiank, W. Mahoney, R. G. Osifchin and R. Reifengerger, *Science* 272, 1323 (1996).
10. C. A. Mirkin, R. L. Letsinger, R. C. Mucic and J. Storho, *Nature* 382, 607 (1996).
11. A. P. Alivisatos, K. P. Johnsson, X. Peng, T. E. Wilson, C. J. Loweth, M. P. Bruchez and P. G. Schultz, *Nature* 382, 609 (1996).
12. J. J. Zhao, X. S. Chen, G. H. Wang, *Phys. Lett. A* 189, 223 (1994).
13. H. Handschuh, G. Gantefor, P. S. Bechthold and W. Eber-

14. I.L. Garzon and A. Posada-Amarilla, Phys. Rev. B 54, 11796 (1996).
15. O.D. Haberkant, S.C. Chung, M. Stener and N. Rosch, J. Chem. Phys. 106, 5189 (1997).
16. J. Wang, G. Wang and J. Zhao, Phys. Rev. B 66, manuscript # BM A 8242, to be published Aug. 15, 2002.
17. I.L. Garzon, K. Michaelian, M.R. Beltran, A. Posada-Amarilla, P. Ordejón, E. Artacho, D. Sanchez-Portal and J.M. Soler, Phys Rev Lett. 81, 1600 (1998).
18. J.L. BelBruno, Heteroatom. Chem. 9, 651 (1998).
19. R.N. Barnett, C.L. Cleveland, H. Hakkinen, W.D. Luedtke, C. Yannouleas and U. Landman, Eur. Phys. J. D 9, 95 (1999).
20. J.M. Soler, M.R. Beltran, K. Michaelian, I.L. Garzon, P. Ordejón, D. Sanchez-Portal and E. Artacho, Phys. Rev. B 61, 5771 (2000).
21. N.T. Wilson and R.L. Johnston, Eur. Phys. J. D 12, 161 (2000).
22. T. Li, S. Yin, Y. Ji, G. Wang and J. Zhao, Phys. Lett. A 267, 403 (2000).
23. H. Hakkinen and U. Landman, Phys. Rev. B 62, 2287 (2000).
24. H. Gronbeck and W. Andreoni, Chem. Phys. 262, 1 (2000).
25. A.H. Romero, A. Castro and A. Rubio, to be published.
26. M.W. Mathews, R.J. Beuhler, M. Ledbetter and L. Friedman, J. Phys. Chem. 90, 251 (1986).
27. P.M. Echenuque, J.R. Manson and R.H. Ritchie, Phys. Rev. Lett. 64, 1413 (1990).
28. M.H. Shapiro and T.A. Tombrello, Phys. Rev. Lett. 65, 92
29. M.H. Shapiro and T.A. Tombrello, Nucl. Inst. Meth. 58, 161 (1991).
30. E. Blastein-Barojas and M.R. Zachariah, Phys. Rev. B 45, 4403 (1992).
31. R. Car and M. Parrinello, Phys. Rev. Lett. 55, 2471 (1985); we have used the CPMD code, version 3.5, developed by J. Hutter et al., at MPI für Festkörperforschung and IBM Research Laboratory (1990-2001).
32. J.P. Perdew, K. Burke and M. Ernzerhof, Phys. Rev. Lett. 175, 531 (1990).
33. H. Partridge, C.W. Bauschlicher, S.R. Langhoff, Chem. Phys. Lett. 175, 531 (1990).
34. J.M. Seminario, J.M. Tour, Int. J. Quant. Chem. 65, 749 (1997).
35. N. Troullier and J. Martins, Phys. Rev. B 43, 1993 (1991).
36. M.S. Daw and M.I. Baskes, Phys. Rev. B 29, 6443 (1984).
37. S.M. Foiles, M.I. Baskes and M.S. Daw, Phys. Rev. B 33, 7983 (1986).
38. J.N. Murrell, R.E. Mottram, Mol. Phys. 69, 571 (1990).
39. H. Cox, R.L. Johnston, J.N. Murrell, J. Sol. State Chem. 145, 517 (1999) and references therein.

| C luster  | M ethod | Sym m etry               | E <sub>b</sub> [eV] | R [Å]       | v [Å <sup>3</sup> ] |
|-----------|---------|--------------------------|---------------------|-------------|---------------------|
| 3 atom s  | EA      | C <sub>2v</sub>          | 2.405               | 1.937{2.438 | 3.317               |
|           | CP      | C <sub>2v</sub>          | 2.182               | 2.607{2.753 | 4.225               |
|           | W J     | D <sub>3h</sub>          | 1.759               | 2.780       | 4.133               |
| 4 atom s  | EA      | D <sub>2d</sub>          | 2.313               | 1.904{2.874 | 3.996               |
|           | CP (a)  | D <sub>2d</sub>          | 2.234               | 2.570{3.120 | 5.857               |
|           | CP (b)  | D <sub>2h</sub> (planar) | 2.517               | 2.700       | 2.346               |
|           | CP (c)  | C <sub>2v</sub> (planar) | 2.504               | 2.648       | 29.759              |
|           | W J     | T <sub>d</sub>           | 2.178               | 2.793       | 5.004               |
| 5 atom s  | EA      | O <sub>h</sub>           | 2.685               | 2.507       | 7.287               |
|           | CP (a)  | O <sub>h</sub>           | 2.464               | 2.801       | 4.672               |
|           | CP (b)  | C <sub>2v</sub> (planar) | 2.652               | 2.715       | 7.706               |
|           | W J     | O <sub>h</sub>           | 2.382               | 2.801       | 4.290               |
| 6 atom s  | EA      | O <sub>h</sub>           | 2.825               | 2.536       | 5.767               |
|           | CP (a)  | O <sub>h</sub>           | 2.523               | 2.834       | 8.663               |
|           | CP (b)  | D <sub>3h</sub> (planar) | 2.870               | 2.712       | 4.365               |
|           | W J     | O <sub>h</sub>           | 2.574               | 2.789       | 7.667               |
| 8 atom s  | EA      | D <sub>2d</sub>          | 2.937               | 2.577       | 5.512               |
|           | CP      | D <sub>2d</sub>          | 2.857               | 2.837       | 7.385               |
|           | W J     | D <sub>2d</sub>          | 2.736               | 2.790       | 6.792               |
| 10 atom s | EA      | D <sub>4d</sub>          | 2.999               | 2.594       | 9.794               |
|           | CP      | D <sub>4d</sub>          | 2.914               | 2.829       | 36.225              |
|           | W J     | D <sub>4d</sub>          | 2.837               | 2.778       | 30.854              |
| 12 atom s | EA (a)  | I <sub>h</sub>           | 3.027               | 2.604       | 15.190              |
|           | EA (b)  | C <sub>5v</sub>          | 3.089               | 2.693       | 21.142              |
|           | CP (a)  | C <sub>5v</sub>          | 2.879               | 2.896       | 33.032              |
|           | CP (b)  | D <sub>4h</sub>          | 2.962               | 2.814       | 8.780               |
|           | W J     | I <sub>h</sub>           | 2.886               | 2.776       | 18.395              |